Limnol. Oceanogr., 53(2), 2008, 614–630

Relating phytoplankton photophysiological properties to community structure on large scales

Julia Uitz[1] *and Yannick Huot*
Laboratoire d'Océanographie de Villefranche, CNRS and Université Pierre et Marie Curie, BP 08, 06 238 Villefranche-sur-Mer Cedex, France

Flavienne Bruyant
Dalhousie University, Department of Oceanography, Halifax, Nova Scotia B3H 4J1, Canada

Marcel Babin and Hervé Claustre
Laboratoire d'Océanographie de Villefranche, CNRS and Université Pierre et Marie Curie, BP 08, 06 238 Villefranche-sur-Mer Cedex, France

Abstract

We analyzed a large dataset of simultaneous measurements of phytoplankton pigments, spectral specific absorption coefficient for phytoplankton [a*(λ)], and photosynthesis versus irradiance (P versus E) curve parameters to examine the possible relationships between phytoplankton community structure and photophysiological properties at large spatial scales. Data were collected in various regions, mostly covering the trophic gradient encountered in the world's open ocean. The community composition is described in terms of biomass of three phytoplankton classes, determined using specific biomarker pigments. We present a general empirical model that describes the dependence of algal photophysiology on both the community composition and the relative irradiance within the water column (essentially reflecting photoacclimation). The application of the model to the in situ dataset enables the identification of vertical profiles of photophysiological properties for each phytoplankton class. The class-specific a*(λ) obtained are consistent with results from the literature and with previous models developed for small and large cells, both in terms of the absolute values and the vertical patterns. Similarly, for the class-specific P versus E curve parameters, the magnitude and vertical distribution obtained with this method are coherent with previous observations. Large cells (mainly diatoms) may be more efficient in carbon storage than smaller cells, whereas their yield of light absorption is lower. We anticipate that such photophysiological parameterizations can improve primary production models by providing estimates of primary production that are specific to different phytoplankton classes on large scale.

Estimates of marine primary production on large to global scales rely on the use of primary production models (e.g., Longhurst et al. 1995; Antoine et al. 1996; Behrenfeld et al. 2002*a*). Such models typically incorporate: (1) an estimate of the phytoplankton biomass, usually in the form of the chlorophyll *a* concentration ([Chl *a*], mg m^{-3}); (2) the photosynthetically available irradiance (from 400 to 700 nm; PAR [μmol quanta m^{-2} s^{-1}]); and (3) a relationship expressing changes in photosynthetic efficiency as a function of incident or absorbed irradiance. Although the mathematical description varies from one model to another (Behrenfeld and Falkowski 1997*a*), all models aim at parameterizing the primary production rate (*P*, mg C m^{-2} h^{-1}) as follows

$$P = 12000[\text{Chl}\,a]\ a^{*}\text{PAR}\ \Phi_c(\text{PAR}) \quad (1)$$

where a* is the chlorophyll-specific absorption coefficient of phytoplankton [m^2 (mg Chl *a*)$^{-1}$], Φ_c(PAR) is the irradiance-dependent quantum yield of carbon fixation [mol C (mol quanta)$^{-1}$], and 12000 enables the conversion of moles of quanta into milligrams of carbon.

Equation 1 includes two photophysiological variables: a* and Φ_c(PAR). The relationship between their product, i.e., a* Φ_c(PAR), and the incident PAR is often expressed by a photosynthesis versus irradiance (P vs. E) curve that can be represented by various mathematical formulations (*see, for example,* Falkowski and Raven, 1997), such as

$$\begin{aligned} P^{B} &= 12000 a^{*}\Phi_c(\text{PAR})\text{PAR} \\ &= P^{B}_{max}[1-\exp(-\alpha^{B}\text{PAR}/P^{B}_{max})] \end{aligned} \quad (2)$$

where P^B is the chlorophyll-normalized primary production. At low light, the conversion of absorbed light energy into carbon can be described by the initial slope of this curve [α^B, mg C (mg Chl *a*)$^{-1}$ h^{-1} (μmol quanta m^{-2} s^{-1})$^{-1}$], which equals to the product a* Φ_{cmax} [Φ_{cmax} being the maximum quantum yield of carbon fixation, mol

[1] Present address: Marine Physical Laboratory, Scripps Institution of Oceanography, University of California at San Diego, La Jolla California 92093.

Acknowledgments

Annick Bricaud substantially contributed to the implementation of the database. We thank Bernard Gentili for help with computation aspects. We are also grateful to anonymous reviewers for their constructive comments. The data used in this study were acquired as part of numerous in situ projects that have largely benefited from funding by the PROOF and then the CYBER French programs.

C (mol quanta)$^{-1}$]. At high irradiance, the P versus E curve reaches a maximum value [P^{B}_{max}, mg C (mg Chl *a*)$^{-1}$ h^{-1}], which is independent of light absorption, and only depends on the maximal capacity of the cell to fix carbon.

Whereas fields of Chl *a* and PAR can be estimated on the global scale by means of satellite observations and models, the prediction of the above-mentioned photophysiological variables has remained challenging. Two main approaches have been proposed so far (Behrenfeld et al. 2002*b*). The first one consists in assigning seasonal estimates to the biogeographical provinces defined by Longhurst (Longhurst 1995; Sathyendranath et al. 1995). In practice, however, this method is difficult to handle when dealing with large scales as a relevant set of photophysiological properties needs to be selected for each of the 56 provinces and because of the unnatural spatial discontinuities resulting from the partitioning into provinces. The second approach aims at relating photophysiological properties to one or more environmental factors. Many authors have investigated in the field or in the laboratory the dependence on temperature, nutrients, and/or light of photophysiological variables such as P^{B}_{max} (e.g., Balch and Byrne 1994; Behrenfeld and Falkowski 1997*b*; Behrenfeld et al. 2002*b*), Φ_{cmax} (e.g., Cleveland et al. 1989; Sosik 1996; Sorensen and Siegel 2001), and a* (e.g., Moore et al. 1995; Stramski et al. 2002; Bouman et al. 2003). Some of these studies led to predictive empirical (or semi-empirical) models enabling, for instance, estimates of P^{B}_{max} on the global scale from temperature (Behrenfeld and Falkowski 1997*b*) or from light and nutrients (Behrenfeld et al. 2002*b*).

Although these predictive models are commonly used, they are still a matter of debate and a potential source of error in estimates of primary production (Morel et al. 1996; Behrenfeld and Falkowski 1997*b*; Behrenfeld et al. 2002*a*). Their description is generally consistent with observations on laboratory cultures where only one physico-chemical factor varies. In natural conditions, photophysiological properties are affected by several environmental factors that operate simultaneously. These concurrent forcings lead to a complex photophysiological response that is difficult to predict (Behrenfeld et al. 2002*b*; Claustre et al. 2005). For instance, from laboratory studies and theory, P^{B}_{max} was expected to be primarily regulated by temperature because it is constrained by the enzymatic activity of the Calvin Cycle (Sukenik et al. 1987; Falkowski and Raven 1997). However, P^{B}_{max} has already been reported to decrease at elevated temperatures ($>20^{\circ}$C) due to the concurrent effects of nutrient limitation (Behrenfeld and Falkowski 1997*b*). The effect of temperature on P^{B}_{max} can also be masked by the overwhelming influence of adaptations of species to their environment. Indeed, high values of P^{B}_{max} have previously been found in low-temperature regions such as the Southern Ocean (e.g., Moline and Prézelin 1996; Hiscock et al. 2003), which challenges the temperature hypothesis. In addition, relationships between algal photophysiology and physico-chemical forcings strongly depend on the spatial and temporal scale of interest (Sosik 1996; Claustre et al. 2005). Hence, predictive models established on the basis of field data collected during specific cruises (e.g., in small oceanic regions, during short periods of time) may not be relevant for global scale applications.

Recent papers indicated possible relationships between photophysiological properties and phytoplankton community structure (in terms of size or types of algae) on small to meso-scales (Hashimoto and Shiomoto 2002; Cermeño et al. 2005; Claustre et al. 2005). But only a few have investigated such relationships on larger scales (Bouman et al. 2005 for P^{B}_{max}; Devred et al. 2006 for a*). We propose here to carry out a prospective study in that direction. The rationale for this approach is that the community structure is determined by the same environmental factors (e.g., nutrients, irradiance regime, temperature) that influence the photophysiological response of phytoplankton (Margalef 1978; Cullen et al. 2002). For example, diatoms are preferentially associated with dynamic systems where fresh nutrients are available (e.g., Malone 1980; Goldman 1993), whereas small algae are mostly found in stratified nutrient-depleted regions (e.g., Malone 1980; Chisholm 1992; Partensky et al. 1999*a*). In that sense, the community structure can be seen as an integrator of environmental factors (Claustre et al. 2005). Thus, using the phytoplankton community structure to predict photophysiological properties could effectively be complementary to the use of environmental factors. In turn, because the composition of the autotrophic communities plays a major role in biogeochemical fluxes (e.g., Eppley and Peterson 1979; Legendre and Le Fèvre 1989), obtaining information on the taxonomic specificity of photophysiological properties may improve model description of biogeochemical cycles (Margalef 1965).

The high-performance liquid chromatography (HPLC) technique enables a suite of algal pigments (Chl *a* and accessory pigments) to be determined. These accessory pigments are commonly used as biomarkers of phytoplankton groups (e.g., Gieskes et al. 1988), or size classes (Vidussi et al. 2001; Devred et al. 2006; Uitz et al. 2006) to estimate the community composition. In the frame of the French Joint Global Ocean Flux Study (JGOFS) program, a multitude of measurements of algal pigment concentrations by HPLC and photophysiological properties (i.e., spectral absorption coefficients of algae and P versus E curve parameters) have been collected by our laboratory in a range of oceanic conditions. These data constitute the set required to start investigations on potential relationships between algal photophysiology and community composition on large scale.

Based on the analysis of this extensive dataset, we evaluate the possibility of using the phytoplankton community structure as an indicator of the photophysiological properties. First, our dataset is submitted to principal component analysis to identify which factors (biological and environmental) influence algal photophysiological properties. According to the results of this preliminary study, we propose a hybrid model that accounts for the dependence of phytoplankton photophysiology on both community structure and relative irradiance within the water column. This model enables the identification of vertical profiles of photophysiological

Table 1. Information concerning the cruises represented in databases P-E and A: geographic location, period of the cruise, and number of samples for each cruise in each database. The range of the surface Chl *a* concentration, $[\text{Chl } a]_{\text{surf}}$ (mg m^{-3}), is also given as an indicator of the trophic status.

Cruise	Location	Period	$[\text{Chl } a]_{\text{surf}}$ range (mg m^{-3})	Dataset P-E	Dataset A
EUMELI 3	Tropical North Atlantic	Oct 1991	0.073–0.340	–	28
EUMELI 4	Tropical North Atlantic	May–Jun 1992	0.044–2.016	65	–
FLUPAC	Equatorial and subequatorial Pacific	Sep–Oct 1994	0.039–0.236	–	38
OLIPAC	Equatorial and subequatorial Pacific	Nov 1994	0.033–0.208	129	125
MINOS	Eastern and western Mediterranean	May 1996	0.048–0.187	9	64
ALMOFRONT 2	Alboran Sea	Dec 1997 and Jan 1998	0.202–1.185	–	304
PROSOPE	Morocco upwelling, eastern and western Mediterranean	Sep–Oct 1999	0.029–2.788	125	351
POMME 1	North Atlantic	Feb–Mar 2001	0.168–0.669	118	530
POMME 2	North Atlantic	Mar–May 2001	0.375–1.430	137	595
POMME 3	North Atlantic	Aug–Oct 2001	0.049–0.227	75	444
BENCAL	Benguela upwelling	Oct 2002	0.243–28.737	–	60
BIOSOPE	Tropical and subtropical south Pacific	Oct–Dec 2004	0.018–1.483	244	268
				902	2807

properties specific to different phytoplankton (pigment-based) types.

Material and methods

Data sampling—The present study relies on the analysis of two extensive databases. The first database comprises simultaneous measurements of algal pigment concentrations, P versus E curve parameters, mean chlorophyll specific absorption coefficient of phytoplankton [$\bar{a}^*$, m^2 (mg Chl $a)^{-1}$], maximum quantum yield for carbon fixation [Φ_{cmax}, mol C (mol quanta)$^{-1}$], temperature (T, °C), and concentrations of nitrates or nitrates plus nitrites, depending on data availability ([Nut], μmol L^{-1}). The P versus E parameters were all determined from experiments carried out in identical conditions (by using the same equipment), which enables the parameters obtained from the different field campaigns to be safely compared. From the initial database including 1,089 samples, we rejected samples with no simultaneous specific absorption coefficient of phytoplankton, or when Φ_{cmax} was greater than the theoretical maximum of 0.125 mol C (mol quanta)$^{-1}$. A one-by-one visual inspection of the vertical profiles of P versus E curve parameters enabled the identification and removal of data points showing evident failure in the P versus E experiment. In anticipation of further analysis, we kept exclusively data sampled between the surface and 1.5 times the euphotic zone depth, so as to remove the potential effect of samples collected at depth for which photophysiological measurements are generally less accurate. At the end of this procedure, the database comprises 902 samples. It will be used to (1) examine the dependence of algal photophysiology on biological and environmental variables (by performing principal component analysis), and (2) analyze the relationships between community composition and P versus E curve parameters. This database will be called "P-E" hereafter (*see* Table 1 for further information).

The second database was compiled and used by Bricaud et al. (2004) and includes additional data collected during the Biogeochemistry and Optics South Pacific Experiment (BIOSOPE) cruise (Table 1). As for the P-E database, samples located below 1.5 times the euphotic layer depth were disregarded. This provided 2,807 simultaneous measurements of phytoplankton pigments and spectral specific absorption coefficients [$a^*(\lambda)$], which will be used to examine the relationships between the phytoplankton community composition and the specific absorption spectra. This database will be called "A."

Both databases include numerous samples collected exclusively in open ocean waters. Data originate from the Mediterranean Sea, the North Atlantic Ocean, and the Equatorial and South Pacific Oceans (Fig. 1). They cover most of the trophic conditions encountered in oceanic regions, from the most oligotrophic waters of the South Pacific Gyre (surface Chl *a* concentration of 0.02 mg m^{-3}) to the eutrophic waters associated with the Moroccan upwelling (surface Chl *a* concentration of 2.8 mg m^{-3} for database P-E), or with the Benguela upwelling (surface Chl *a* of 28.7 mg m^{-3} for database A).

Pigments, algal specific absorption, and P versus E curve parameters measurements—Concentrations of Chl *a* and accessory pigments were measured by HPLC, following the procedure described by Claustre and Marty (1995) for the EUtrophic, MEsotrophic, and oLIgotrophic (EUMELI) cruises, Van Heukelem and Thomas (2001) for the BIOSOPE cruise, and Vidussi et al. (1996) for all other cruises. In what follows, [Chl *a*] will refer to the concentration of the total Chl *a*, which is the sum of the concentrations of the Chl *a*, divinyl-Chl *a*, and chlorophyllide *a*.

The method used for phytoplankton specific absorption measurements is detailed in the works of Bricaud et al. (1998, 2004).

The P versus E experiments were carried out following the method described by Babin et al. (1994, 1996). For each

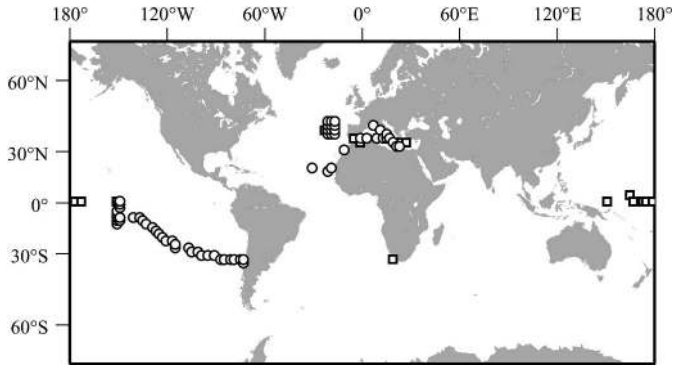

Fig. 1. Location of the stations where the data included in databases A and P-E were collected. Circles indicate samples comprised both in databases A and P-E. Squares correspond to samples comprised in database A exclusively.

P versus E curve, α^B and P^B_{max} were determined by fitting the model of Platt et al. (1980) to the experimental P^B versus PAR data. This procedure avoids discrepancies resulting from the dependence of the P versus E curve parameters on the choice of the model (Frenette et al. 1993). The saturation parameter (E_k, μmol quanta m^{-2} s^{-1}) was derived from

$$E_k = P^B_{max}/\alpha^B \quad (3)$$

The maximum quantum yield for carbon fixation was calculated as follows:

$$\Phi_{cmax} = \alpha^B/12000\,\bar{a}^* \quad (4)$$

where 12000 is the molar weight (mg) of carbon, and $\bar{a}^*$ (m^2 (mg Chl a)$^{-1}$) is the mean chlorophyll-specific absorption coefficient of algae, weighted by the spectral distribution [E(λ)] of the PAR used during the P versus E experiments.

$$\bar{a}^* = \frac{\int_{400}^{700} a^*(\lambda)E(\lambda)d\lambda}{\int_{400}^{700} E(\lambda)d\lambda} \quad (5)$$

Euphotic layer depth and hydrological regime determination—The euphotic depth (Z_{eu}), defined as the depth where the PAR is reduced to 1% of its surface value, has not been systematically measured. Thus, for each station considered in the present study, it has been obtained from the vertical profile of [Chl a] by using the model of Morel and Maritorena (2001). We define the surface layer as the layer delimited by the so-called penetration depth (Z_{pd}), calculated as $Z_{eu}/4.6$. We use the index z/Z_{eu} as an indicator of the relative available irradiance at the sampling depth.

Samples from databases P-E and A are discriminated into two basic hydrological categories: stratified waters (i.e., Z_{eu} is deeper than the mixed layer depth, Z_m), and well-mixed waters (i.e., Z_{eu} is shallower than Z_m). The Z_m has been systematically extracted from a monthly global climatology (de Boyer Montégut et al. 2004), which was sufficient for this rough categorization (*see* Uitz et al. 2006).

Using pigment measurements to derive biological variables—Phytoplankton community composition: The phytoplankton community composition can be described based on accessory pigments. Here we used the method developed by Claustre (1994) and Vidussi et al. (2001), and recently improved by Uitz et al. (2006), to estimate the contribution of three pigment-based size classes to the total algal biomass. Basically, seven diagnostic pigments are selected as biomarkers of specific taxa. These taxa are gathered into three size classes, i.e., micro-, nano-, and picophytoplankton, according to the average size of the organisms (*see* table 1 in Vidussi et al. 2001 and relevant references therein). The fractions of these three pigment-based size classes relative to the total algal biomass are calculated from

$$f_{micro} = (1.41[\text{fucoxanthin}] + 1.41[\text{peridinin}])/\text{wDP} \quad (6)$$

$$f_{nano} = (0.60[\text{alloxanthin}] + 0.35[19' - \text{BF}] + 1.27[19' - \text{HF}])/\text{wDP} \quad (7)$$

$$f_{pico} = (0.86[\text{zeaxanthin}] + 1.01[\text{Chl}\,b + \text{divinyl} - \text{Chl}\,b])/\text{wDP} \quad (8)$$

where wDP is the weighted sum of the concentrations of the seven diagnostic pigments

$$\begin{aligned}\text{wDP} = {} & 1.41[\text{fucoxanthin}] + 1.41[\text{peridinin}] \\ & + 0.60[\text{alloxanthin}] + 0.35[19' - \text{BF}] \\ & + 1.27[19' - \text{HF}] + 0.86[\text{zeaxanthin}] \\ & + 1.01[\text{Chl}\,b + \text{divinyl} - \text{Chl}\,b]\end{aligned} \quad (9)$$

The coefficients used in Eqs. 6–9 represent average ratios between [Chl a] and the concentration of each diagnostic pigment; they were determined by multiple regression analysis performed on a global dataset (Uitz et al. 2006). The [Chl a] associated with each class can be computed as follows:

$$[\text{Chl}\,a]_{micro} = f_{micro} \times [\text{Chl}\,a] \quad (10)$$

$$[\text{Chl}\,a]_{nano} = f_{nano} \times [\text{Chl}\,a] \quad (11)$$

$$[\text{Chl}\,a]_{pico} = f_{pico} \times [\text{Chl}\,a] \quad (12)$$

where $f_{micro} + f_{nano} + f_{pico} = 1$.

As already acknowledged (Vidussi et al. 2001; Uitz et al. 2006), this method might sometimes lead to discrepancies as some diagnostic pigments can be shared by various phytoplankton groups (e.g., fucoxanthin, the main carotenoid of diatoms, may be present in some nanoplankton prymnesiophytes), and some groups may spread over a wide size range (e.g., equatorial diatoms may not fall into the micro-, but in the nano-size range). Despite these limita-

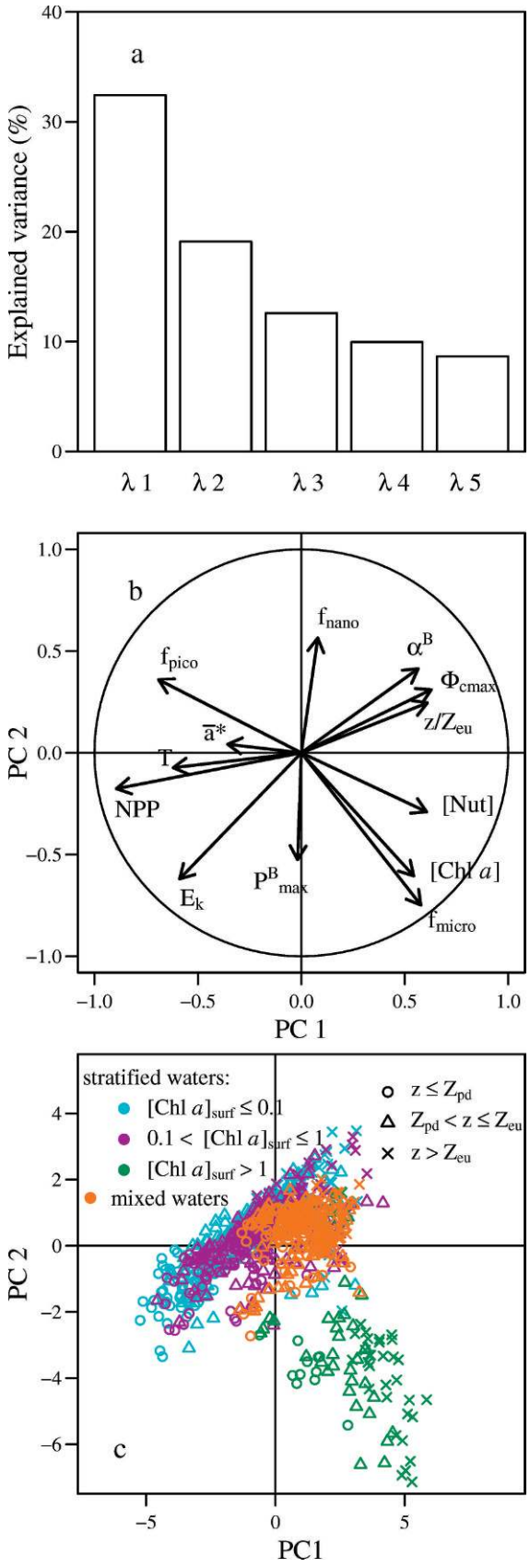

Fig. 2. Graphical representation of PCA results: (a) eigenvalues (λ) associated with the first five principal axes of the data matrix P-E, (b) correlation circle in the plane formed by the two first principal components (PC1 × PC2), and (c) projection of the individual samples. On panel c, colors are according to trophic status, and symbols are according to optical depth. Samples are discriminated according to the hydrological regime: Well-mixed waters (i.e., $Z_{eu} < Z_m$; orange symbols) or stratified waters (i.e., $Z_{eu} \geq Z_m$; other symbols). The range of the surface Chl *a* concentration ($[Chl\ a]_{surf}$, mg m^{-3}) is indicated for stratified waters only; the range of the sampling depth is indicated for both stratified and mixed waters. The three classes based on $[Chl\ a]_{surf}$ (i.e., $[Chl\ a]_{surf} \leq 0.1$ mg m^{-3}, 0.1 mg $m^{-3} < [Chl\ a]_{surf} \leq 1$ mg m^{-3}, and $[Chl\ a]_{surf} > 1$ mg m^{-3}) are very rough indexes of the trophic status of the environment: Rather oligotrophic (turquoise symbols), mesotrophic (purple symbols), or eutrophic (green symbols).

tions, this approach characterizes the taxonomic community composition of the entire phytoplankton biomass and simultaneously yields reasonable information on its size structure (Bricaud et al. 2004), e.g., micro-, nano-, and picophytoplankton mainly include diatoms, prymnesiophytes, and prokaryotes, respectively.

Non-photosynthetic pigment index: We use the non-photosynthetic pigment (NPP) index proposed by Babin et al. (1996), defined as the ratio of the concentrations of non-photosynthetic pigments (i.e., zeaxanthin, diadinoxanthin, diatoxanthin, and β-carotene) to the concentrations of total pigments (i.e., non-photosynthetic chlorophylls and photosynthetic carotenoids; Bidigare et al. 1990). Because these pigments are group-specific, the NPP index is controlled by both phytoplankton community composition and photoacclimation processes.

Photophysiological properties versus environmental and biological variables

The possible dependence of algal photophysiology upon biological and environmental variables is examined by means of a principal component analysis (PCA) performed on the P-E database. In the present study, the PCA enables a visualization of the similarities and differences between the samples of this database, as well as the correlations between the variables of interest (i.e., photophysiological, biological, and environmental).

The data matrix is composed of 902 individual samples and 12 variables. Those are E_k, P^B_{max}, α^B, $\bar{a}^*$, and Φ_{cmax} for the photophysiological variables; [Chl *a*], f_{micro}, f_{nano}, f_{pico}, and the NPP index for the biological variables; T, [Nut], and z/Z_{eu} for the environmental variables. Before the analysis, the data were mean-centered and normalized to one standard deviation so that variables having different dispersions, or measured in different units, can be compared. The eigenvalues of the data matrix show that the first two principal components account only for more than 50% of the variability of the dataset (Fig. 2a). We will nevertheless limit our analysis to the first factorial plane (PC1 × PC2) as it is sufficient for our purpose.

Table 2. Mean (±SD) photophysiological variables (E_k, P^B_{max}, α^B, $\bar{a}^*$, and Φ_{cmax}) for the three trophic classes of stratified waters and for mixed waters in three distinct layers of the water column: 0–Z_{pd}, Z_{pd}–Z_{eu}, and >Z_{eu}. Also shown is the statistical significance (p) of the differences between the three layers of the water column (Kruskal-Wallis test): *$p < 0.05$; **$p < 0.01$; ***$p < 0.001$; ns: not significant.

		Stratified waters [Chl a]$_{surf} \leq 0.1$ $n = 408$ mean±SD	K-W	$0.1 <$ [Chl a]$_{surf} \leq 1$ $n = 186$ mean±SD	K-W	[Chl a]$_{surf} > 1$ $n = 68$ mean±SD	K-W	Mixed waters $n = 240$ mean±SD	K-W
E_k	0–Z_{pd}	238±100	***	171±98	***	138±32	ns	74±58	***
	Z_{pd}–Z_{eu}	96±79		87±70		98±58		59±44	
	>Z_{eu}	22±13		30±15		111±61		43±11	
P^B_{max}	0–Z_{pd}	2.81±1.46	***	3.50±1.44	***	3.68±0.78	*	2.91±1.71	**
	Z_{pd}–Z_{eu}	1.58±1.17		2.12±1.29		2.71±1.40		2.45±1.15	
	>Z_{eu}	0.89±0.54		1.21±0.87		2.57±1.63		1.96±0.84	
α^B	0–Z_{pd}	0.013±0.006	***	0.026±0.018	**	0.028±0.008	ns	0.045±0.027	ns
	Z_{pd}–Z_{eu}	0.025±0.022		0.032±0.022		0.031±0.015		0.047±0.019	
	>Z_{eu}	0.045±0.025		0.041±0.020		0.023±0.007		0.047±0.020	
$\bar{a}^*$	0–Z_{pd}	0.036±0.012	***	0.028±0.009	*	0.024±0.004	ns	0.028±0.007	ns
	Z_{pd}–Z_{eu}	0.028±0.009		0.026±0.008		0.020±0.007		0.028±0.007	
	>Z_{eu}	0.024±0.009		0.022±0.006		0.020±0.012		0.029±0.006	
Φ_{cmax}	0–Z_{pd}	0.009±0.005	***	0.023±0.015	***	0.027±0.008	ns	0.038±0.019	ns
	Z_{pd}–Z_{eu}	0.023±0.024		0.031±0.022		0.038±0.016		0.040±0.017	
	>Z_{eu}	0.045±0.028		0.048±0.038		0.036±0.019		0.038±0.015	

Representation of individual samples—The main variables contributing to the formation of the first principal component (PC1) are the NPP index ($r^2 = 0.80$), f_{pico} ($r^2 = 0.48$), z/Z_{eu} ($r^2 = 0.37$), and E_k ($r^2 = 0.35$). The PC1 is thus primarily influenced by the photoacclimation status of the algae and by the community composition (Fig. 2b). The main variables that form the second principal component (PC2) are f_{micro} ($r^2 = 0.56$), and [Chl a], f_{nano}, and E_k at nearly equivalent parts ($r^2 = 0.37$, 0.32, and 0.38, respectively). Those contributions suggest that PC2 mostly represents the community composition, the trophic status, and photoacclimation processes.

We begin by looking at the samples projected in the factorial plane formed by PC1 and PC2 (Fig. 2c). For convenience in interpretation, samples collected in stratified waters are separated into three classes defined by successive intervals of surface Chl a concentration ([Chl a]$_{surf}$): [Chl a]$_{surf} \leq 0.1$ mg m^{-3}, 0.1 mg m^{-3} < [Chl a]$_{surf}$ ≤ 1 mg m^{-3}, and [Chl a]$_{surf} > 1$ mg m^{-3}.

The data points are divided into two main groups according to the community composition and the trophic status. On the right-bottom part of the plot, one finds samples collected in eutrophic regimes, mainly in upwelling systems, characterized by high values of [Chl a] and f_{micro}. The other samples, characterized by lower f_{micro} and chlorophyll biomass, originate from either oligotrophic or mesotrophic environments. Samples collected in stratified oligotrophic regions (e.g., Mediterranean Sea) are characterized by high values of f_{pico} and NPP index. Most of the samples collected in stratified mesotrophic situations (e.g., Equatorial Pacific) behave similarly. The others share the same features as those originating from well-mixed waters (e.g., North Atlantic in the beginning of spring), i.e., intermediate [Chl a] levels and dominance of nanophytoplankton. Well-mixed water samples were essentially collected in oligotrophic and mesotrophic environments (North Atlantic during winter and early spring) and thus form a unique cluster.

Data points collected in stratified oligotrophic situations, and to a lesser extent those collected in stratified mesotrophic situations, are discriminated as a function of the sampling depth. One finds samples collected within the surface layer ($z \leq Z_{pd}$) on the left side of PC1, below PC2, whereas those collected below the euphotic zone ($z > Z_{eu}$) are distributed on the right side of PC1, above PC2. In these systems, all of the photophysiological variables show significant differences between the three layers of the water column, i.e., 0–Z_{pd}, Z_{pd}–Z_{eu}, and >Z_{eu} (Kruskal-Wallis test, $p < 0.001$; Table 2). This ''depth effect'' tends to vanish for high [Chl a] samples as well as for samples typical of well-mixed waters. In these situations, differences between the three layers of the water column were insignificant for most of the photophysiological variables (Kruskal-Wallis test; Table 2).

Correlations between photophysiological, biological, and environmental variables—Correlation between variables are studied by examining the correlation matrix (Table 3) and the correlation circles in the factorial planes formed by PC1 and PC2 axes (Fig. 2b) and by PC1 and PC3 axes (where P^B_{max} is better represented; not shown here).

The variables P^B_{max} and $\bar{a}^*$ appeared to be controlled mostly by biological factors and by z/Z_{eu}. P^B_{max} is positively correlated to [Chl a] and f_{micro} and negatively to f_{pico} and z/Z_{eu}. The $\bar{a}^*$ is negatively correlated to [Chl a], f_{micro}, and z/Z_{eu} and positively to f_{pico} and NPP.

The variables α^B and E_k are mostly controlled by irradiance-related factors. Notably, α^B is positively correlated to z/Z_{eu} and negatively correlated to NPP and T, whereas E_k is positively correlated to NPP and T and negatively to z/Z_{eu}. Apart from α^B, from which it is calculated, Φ_{cmax} shows significant correlations to NPP and

Table 3. Correlation matrix. Linear correlation coefficients (r) between photophysiological, biological, and environmental variables for database P-E. Only values which are significant at the $p < 0.001$ level are reported. Correlation coefficients between the photophysiological variables and the two other types of variables (i.e., biological and environmental) are in bold.

	E_k	P^B_{max}	α^B	$\bar{a}^*$	Φ_{cmax}	[Chl a]	f_{micro}	f_{nano}	f_{pico}	NPP	T	[Nut]	z/Z_{eu}
E_k	1.000												
P^B_{max}	0.508	1.000											
α^B	−0.500	0.206	1.000										
$\bar{a}^*$	0.177	0.193		1.000									
Φ_{cmax}	−0.451	0.109	0.796	−0.364	1.000								
[Chl a]		**0.290**		**−0.301**	**0.214**	1.000							
f_{micro}		**0.258**		**−0.214**	**0.106**	0.688	1.000						
f_{nano}	**−0.234**		**0.229**		**0.165**	−0.268	−0.470	1.000					
f_{pico}	**0.116**	**−0.231**	**−0.176**	**0.261**	**−0.247**	−0.531	−0.708	−0.291	1.000				
NPP	**0.604**	**0.138**	**−0.468**	**0.283**	**−0.486**	−0.375	−0.359	−0.221	0.566	1.000			
T	**0.378**		**−0.369**	**−0.139**	**−0.150**	−0.291	−0.239		0.338	0.629	1.000		
[Nut]	**−0.201**		**0.116**	**−0.123**	**0.158**	0.292	0.540	−0.242	−0.392	−0.462	−0.380	1.000	
z/Z_{eu}	**−0.465**	**−0.320**	**0.254**	**−0.220**	**0.317**		0.233		−0.220	−0.586	−0.305	0.412	1.000

z/Z_{eu}. The correlation matrix (Table 3) reveals that α^B and Φ_{cmax} are also influenced by biological factors, e.g., f_{nano} in the case of α^B and f_{pico} in the case of Φ_{cmax} (the correlation level is comparable with that observed between α^B or Φ_{cmax} and z/Z_{eu}; t-test, $p < 0.001$).

Preliminary discussion—The present analysis indicates that almost all photophysiological properties covary with NPP, which is controlled by both photoacclimation processes and community composition, and with the relative irradiance at the sampling depth, here indexed on z/Z_{eu}. Some of the properties, primarily P^B_{max} and $\bar{a}^*$, also depend on the proportion of phytoplankton classes and on [Chl a]. This analysis thus suggests that, beside the community structure, the relative irradiance within the water column is an important factor to consider for the prediction of photophysiological properties. This is particularly important in stratified oligotrophic and mesotrophic systems. Indeed, the present analysis indicates that the index z/Z_{eu} significantly influences algal photophysiology in these systems, whereas its effect is considerably reduced in eutrophic conditions and in well-mixed waters. As mentioned above and generally acknowledged, pico-, nano-, and microphytoplankton are the dominant group in oligotrophic, mesotrophic, and eutrophic situations, respectively (e.g., Malone 1980; Chisholm 1992; Goldman 1993). It follows that the photophysiological properties specific to pico- and nanophytoplankton are expected to display marked vertical patterns, whereas those associated with microphytoplankton should be more homogeneous within the water column.

Relating photophysiological properties to phytoplankton community composition

Claustre et al. (2005) used a multiple regression analysis to estimate the contribution of each of the three phytoplankton pigment-based size classes to various photophysiological parameters. With this approach in mind, we propose a new model that accounts for both the community structure as well as the z/Z_{eu}-dependence of the algal photophysiological properties:

$$\begin{aligned} x^* = (1/[\text{Chl}\,a])([\text{Chl}\,a]_{micro}\, x^*_{micro}(0) e^{-s_{micro}\, z/Z_{eu}} \\ + [\text{Chl}\,a]_{nano}\, x^*_{nano}(0) e^{-s_{nano}\, z/Z_{eu}} \\ + [\text{Chl}\,a]_{pico}\, x^*_{pico}(0) e^{-s_{pico}\, z/Z_{eu}}) \end{aligned} \quad (13)$$

In Eq. 13, x* stands for any chlorophyll-normalized parameter (a^*, α^B, or P^B_{max}); $x^*_{micro}(0)$, $x^*_{nano}(0)$, and $x^*_{pico}(0)$ represent any chlorophyll-normalized parameter at the surface, specific to micro-, nano-, and picophytoplankton, respectively; and s_{micro}, s_{nano}, and s_{pico} are the slopes describing the variations of the photophysiological parameters along the vertical z/Z_{eu} axis.

The present formulation assumes that the photophysiological properties of a phytoplankton population can be derived from the additive combination of the photophysiological properties specific to three phytoplankton classes, provided that the biomass contribution of these classes and the z/Z_{eu} index are known. For each phytoplankton class, the model implies a surface specific value and a depth dependence, reflecting the effect of photoacclimation.

Such hypotheses appear reasonable in the case of the phytoplankton-specific absorption coefficient, which is an additive property and can be described as the sum of the absorption by the different components of the phytoplankton population, the pigment-based size classes in the present case. Phytoplankton-specific absorption is known to be primarily determined by pigment composition and pigment packaging, which is strongly influenced by cell size (e.g., Morel and Bricaud 1981; Hoepffner and Sathyendranath 1991; Lohrenz et al. 2003). Thus, considering that each phytoplankton pigment-based size class is characterized by an average pigmentation and size, each class should have a different surface specific absorption spectrum.

The additive property of the other photophysiological parameters has, to our best knowledge, never been verified, but it stands to logic that unless there is interaction between two populations, their respective carbon uptake will sum

up. In addition to community structure (e.g., Côté and Platt 1983) and photoacclimation (e.g., Babin et al. 1996) related variability, photosynthetic parameters are reckoned to be subject to physico-chemical factors (nutrient status, temperature). The conditions leading to the dominance of certain taxa are also different (e.g., Margalef 1978; Cullen et al. 2002), and cell size affects their ability to compete (Kiorbe 1993). Furthermore, the effect of cell size on the photophysiological parameters has also been shown (e.g., Cermeño et al. 2005). Thus, one can expect that the class-specific surface values featured in the model would partially integrate the influence of those diverse biological and physico-chemical factors, which in effect cannot be discriminated. Hence, the present approach will be first applied to the phytoplankton absorption spectra before being tested using the photosynthetic parameters P^{B}_{max} and α^{B}.

In practice, Eq. 13 is fitted by using a nonlinear least square method (Gaussian-Newton algorithm; R software, http://www.R-project.org) to experimental data of x* (dependent variable) and of [Chl *a*] associated with the three phytoplankton classes (independent variables; a weak correlation of 18% is observed between $[\text{Chl } a]_{nano}$ and $[\text{Chl } a]_{pico}$ for database A and of 15% for database P-E, whereas the two other paired variables are insignificantly correlated). $x^{*}_{micro}(0)$, $x^{*}_{nano}(0)$, $x^{*}_{pico}(0)$, s_{micro}, s_{nano}, and s_{pico} are the unknown parameters.

Only data collected in stratified waters were considered for this analysis (i.e., $n = 1{,}585$ for database A, and $n = 615$ for database P-E). The rationale for this separation was to prevent the vertical patterns displayed by algal photophysiological properties in stratified waters (e.g., Babin et al 1996) to be masked by the uniform distribution typical of well-mixed waters (e.g., Marañon and Holligan 1999).

Spectral specific absorption of algae—The proposed model is applied to the phytoplankton specific absorption spectra of database A. Equation 13 is fitted to data for each available wavelength (i.e., each 2 nm in the range 400–700 nm) to obtain a complete specific absorption spectrum for each phytoplankton class.

The resulting parameters are given in Web Appendix 1 (www.aslo.org/lo/toc/vol_53/issue_2/0614a1.pdf), along with their standard error and statistical significance. The spectra retrieved for each phytoplankton class and for three depths ($z/Z_{eu} = 0$, $z/Z_{eu} = 0.5$, and $z/Z_{eu} = 1$) are displayed on Fig. 3a; the spectra normalized by their maximum value are also presented on Fig. 3b.

All of the specific absorption spectra exhibit the typical peaks of the Chl *a* (at 440 nm and 676 nm). Specific absorption spectra associated with microphytoplankton exhibit the peaks of fucoxanthin (at 440 and 460 nm) and peridinin (around 480 nm). They also show the peak of phaeopigments (at 410 nm). These degradation pigments are typical of eutrophic waters where microphytoplankton are usually found. Specific absorption spectra of nano- and picophytoplankton are also characterized by the peaks of the corresponding biomarker pigments. On the one hand, whatever the considered depth, microphytoplankton show the lowest absorption coefficients of the three classes due to

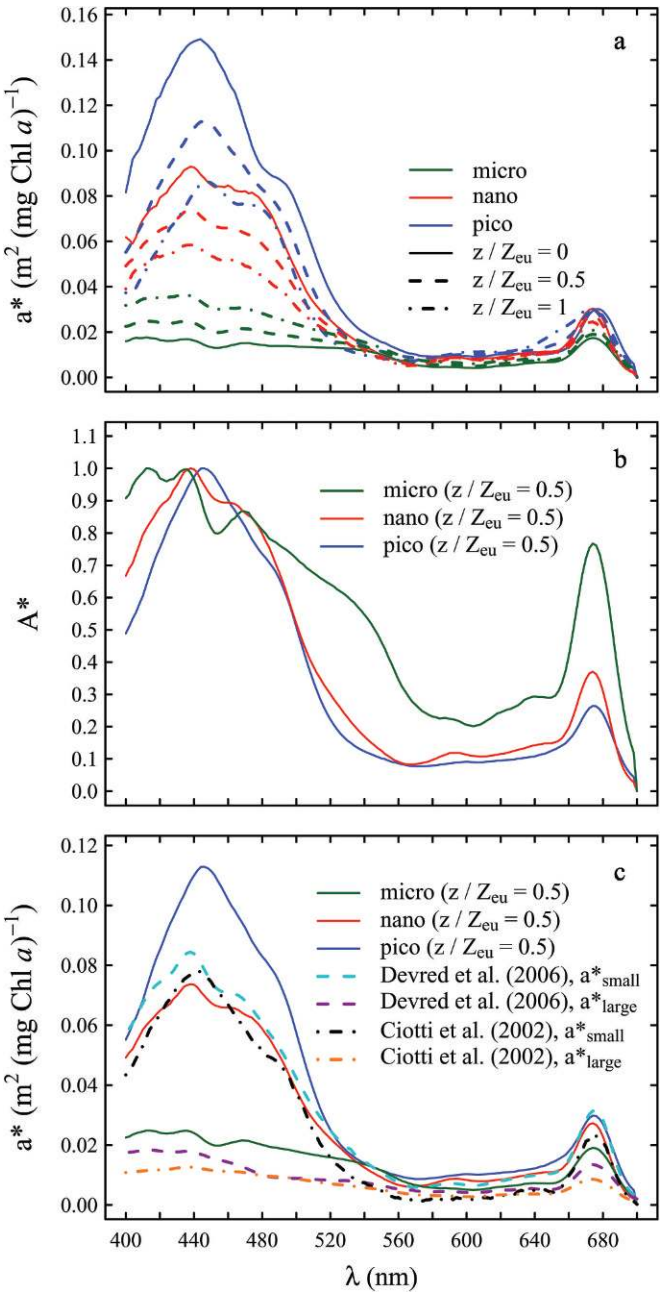

Fig. 3. (a) Spectra of the absorption coefficient [a*(λ)], and (b) of the absorption coefficient normalized by the maximum value (A*) for each pigment-based size class: Micro- (green), nano- (red), and picophytoplankton (blue), and for three different depths: $z/Z_{eu} = 0$ (solid lines), $z/Z_{eu} = 0.5$ (dashed lines), and $z/Z_{eu} = 1$ (dotted lines). Spectra are computed using the parameters listed in Web Appendix 1. (c) Comparison of the spectra obtained for $z/Z_{eu} = 0.5$ for the three phytoplankton classes (solid lines), reproduced from panel a, to the spectra obtained from the model of Devred et al. (2006) (dashed lines) for small (turquoise) and large (purple) cells and from that of Ciotti et al. (2002) (dotted lines) for small (black) and large (orange) cells. The latter were reproduced from the data provided in table 3 in Devred et al. (2006), and in table 3 in Ciotti et al. (2002).

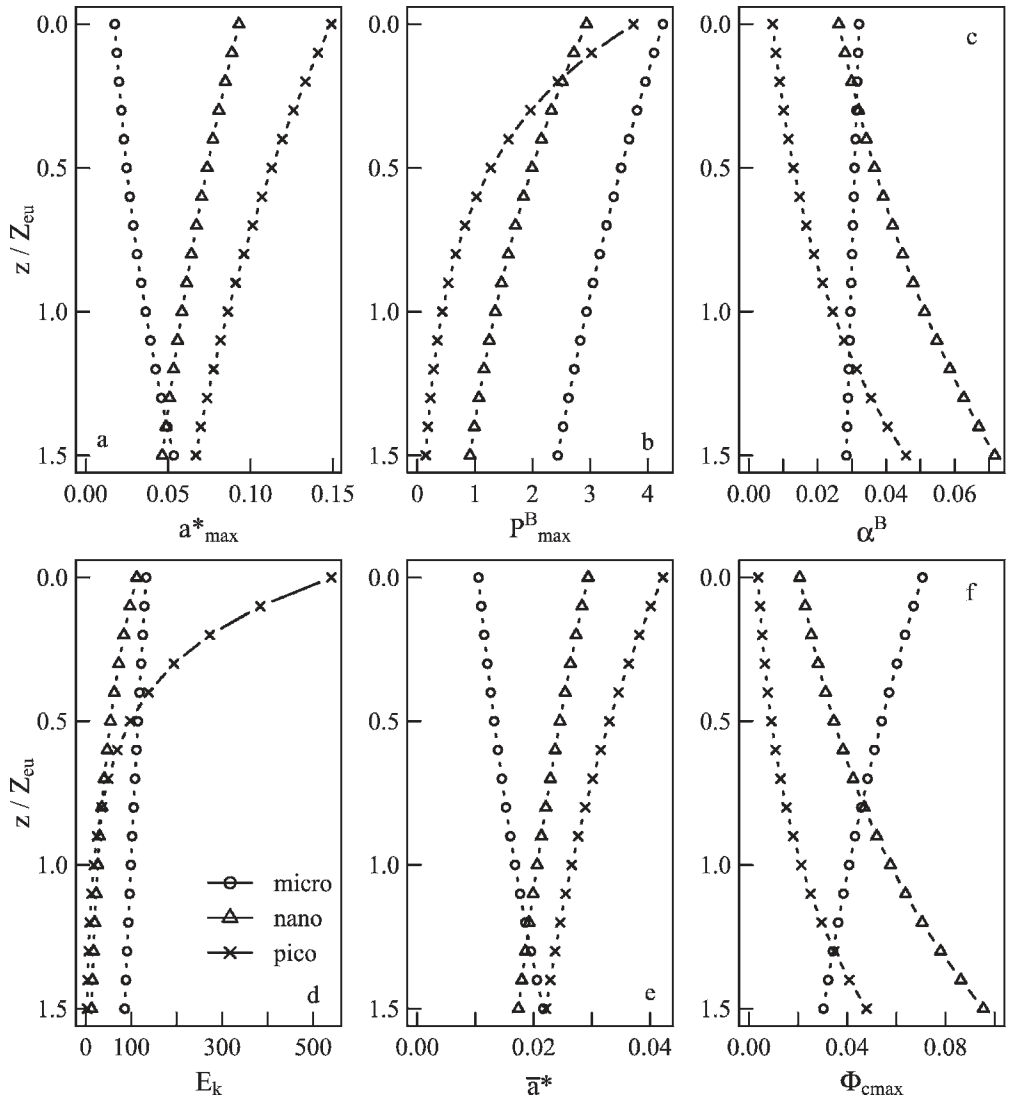

Fig. 4. Vertical profiles of photophysiological parameters specific to the three pigment-based size classes: micro- (circles), nano- (triangles), and picophytoplankton (crosses). (a) a^*_{max} [m^2 (mg Chl *a*)$^{-1}$] is computed from the parameters listed in Web Appendix 1, and (b) P^B_{max} [mg C (mg Chl *a*)$^{-1}$ h^{-1}] and (c) α^B [mg C (mg Chl *a*)$^{-1}$ h^{-1} (μmol quanta m^{-2} s^{-1})$^{-1}$] from the parameters in Table 4. (d) E_k (μmol quanta m^{-2} s^{-1}) is derived according Eq. 3, (e) $\bar{a}^*$ [m^2 (mg Chl *a*)$^{-1}$] according Eq. 5, and (f) Φ_{cmax} [mol C (mol quanta)$^{-1}$] according Eq. 4.

the strong package effect occurring in large cells (Morel and Bricaud 1981). On the other hand, picophytoplankton generally display the highest values, resulting from a reduced packaging, as well as from the presence of non-photosynthetic carotenoids such as zeaxanthin or β-carotene that enhance the absorption in the blue part of the spectrum.

Superimposed on differences related to community composition arise strong vertical features. For the three phytoplankton groupings, vertical gradients are more obvious in the blue part of the spectrum than in the red one. Actually, the slopes s_{micro}, s_{nano}, and s_{pico} are significantly different from 0 in the blue, whereas it is not always the case in the red (*see* Web Appendix 1). In the case of nano- and picophytoplankton, a* in the blue band tends to decrease as z/Z_{eu} increases. This trend is especially pronounced for picophytoplankton, the population characteristic of stratified oligotrophic environments (*see also* Fig. 4a). This result is consistent with studies conducted in the laboratory (e.g., Morel et al. 1993; Moore et al. 1995), or in the field (e.g., Babin et al. 1996; Allali et al. 1997). It is related to photoacclimation processes by which algae adjust their pigment stoichiometry and intracellular pigment content to changes in the intensity and spectral quality of the irradiance. It is also due to photoadaptation, which leads to different species being more competent for growth at different depths. For *Prochlorococcus* (Partensky et al. 1993; Lutz et al. 2003), as for *Synechococcus* (Kana et al. 1988; Six et al. 2004), the zeaxanthin to Chl *a* (or divinyl-Chl *a*) ratio is known to increase with PAR, leading

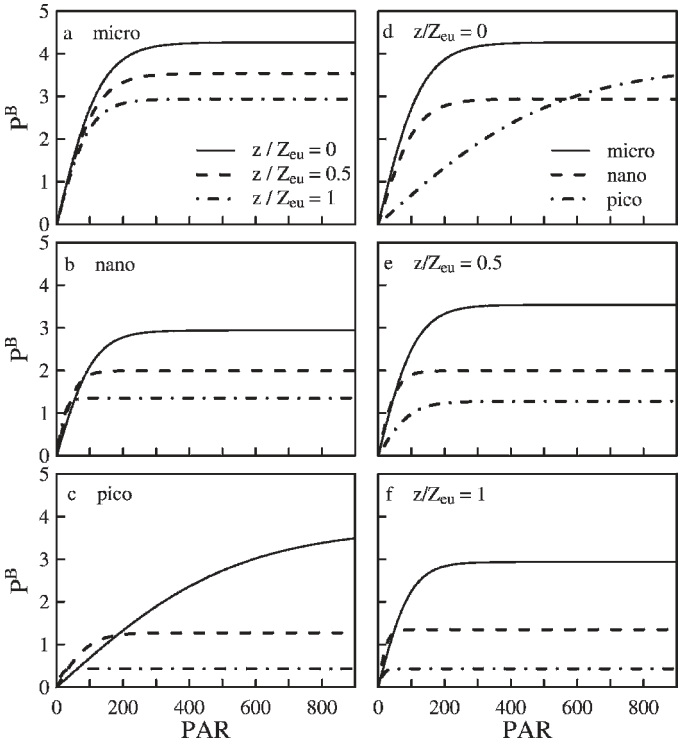

Fig. 5. P^B [mg C (mg Chl a)$^{-1}$ h^{-1}] versus PAR (μmol quanta m^{-2} s^{-1}) curves reconstructed for the three phytoplankton pigment-based size classes for three different depths. (a–c) for each phytoplankton class at $z/Z_{eu} = 0$ (solid lines), $z/Z_{eu} = 0.5$ (dashed lines), and $z/Z_{eu} = 1$ (dotted lines). (d–f) At each depth, for micro- (solid lines), nano- (dashed lines), and picophytoplankton (dotted lines). The curves are reconstructed using the parameters listed in Table 4.

to an increase in the specific absorption coefficient in the blue within the upper layer of the water column. These features may also be related to the occurrence of two (or more) ecotypes of *Prochlorococcus* in the water column, adapted to contrasted PAR levels, and characterized by different accessory pigment contents (Moore and Chisholm 1999; Partensky et al. 1999*b*; Bouman et al. 2006). The opposite vertical gradient is observed for microphytoplankton, for which absorption in the blue part of the spectrum tends to increase with z/Z_{eu} (note that s_{micro} is statistically significant in the blue; Web Appendix 1). This result may be because of a small increase in the concentration of accessory photosynthetic pigments like fucoxanthin in stratified conditions, as already reported in several studies (e.g., Claustre and Marty 1995; Scharek et al. 1999; Gibb et al. 2001) or to a shift toward smaller, less packaged cells at depth.

Recently, Devred et al. (2006) proposed a model to reconstruct specific absorption spectra for small and large cells. Spectra retrieved from their model and from the present model are comparable (Fig. 3c), although we retrieve higher specific absorption coefficients, in particular for picophytoplankton. Indeed, the spectrum of Devred et al. (2006) for small cells is closer to that we obtained for nano- than for picophytoplankton. The same trends are observed when comparing our specific absorption spectra to those from the model of Ciotti et al. (2002) for small and large cells (even though the latter yields slightly lower values than that of Devred et al. for each population; *see* comparison in Devred et al. 2006). In the model of Devred et al. (2006), small cells are treated as a mixture of nano- and picoplankton which could explain the lower specific absorption coefficients they obtained for their small cell population. The differences observed between the results of the Ciotti et al. (2002) model and the present model may be due to the composition of the datasets. Database A includes samples collected in very oligotrophic regions, like the subtropical gyres of the North Atlantic and South Pacific. This could explain the higher specific absorption coefficients obtained here, especially for picophytoplankton in the blue part of the visible spectrum. Eventually, divergences among spectra from the three models may also be due to the different mathematical approaches. The approach adopted here leads to spectra associated with "pure" populations of micro-, nano-, and picophytoplankton, even if these populations rarely, if ever, occur in natural environment.

More generally, the values shown by our specific absorption spectra compare well with the literature. For example, the maximum values (a^*_{max}) retrieved for microphytoplankton [0.018–0.053 m^2 (mg Chl a)$^{-1}$] are consistent with those measured on monospecific laboratory-controlled cultures of diatoms [e.g., 0.015–0.048 m^2 (mg Chl a)$^{-1}$; Sathyendranath et al. 1987; Sakshaug et al. 1989; Finkel 2001]. For nanophytoplankton, a^*_{max} varies within the range 0.046–0.093 m^2 (mg Chl a)$^{-1}$, which is consistent with values observed in the laboratory (e.g., on coccolithophorid culture; Morel and Bricaud 1981), or in mesotrophic nano-dominated environments (e.g., Sosik and Mitchell 1995; Wozniak et al. 2003). Values retrieved for picophytoplankton [0.067–0.149 m^2 (mg Chl a)$^{-1}$] coincide with those obtained on laboratory monospecific cultures of different strains of *Prochlorococcus* [e.g., 0.03–0.190 m^2 (mg Chl a)$^{-1}$; Partensky et al. 1993; Moore et al. 1995] or *Synechococcus* [e.g., 0.065–0.130 m^2 (mg Chl a)$^{-1}$; Morel et al. 1993] grown at contrasted PAR. They also corroborated those observed by Babin et al. (1996) in the oligotrophic tropical North Atlantic at a pico-dominated site [i.e., 0.06–0.160 m^2 (mg Chl a)$^{-1}$ from depth to surface], although the datasets are not completely independent. The relative irradiance-variability observed both in the laboratory and in the field is well reproduced by the present model, which partly accounts for photoacclimation processes by explicitly incorporating the index z/Z_{eu}.

The good agreement between our approach and past methods for retrieving group-specific $a^*(\lambda)$ is an a posteriori validation of the method. We can thus move onto its application to the other photophysiological properties with some degree of confidence.

P versus E curve parameters and maximum quantum yield of carbon fixation—As for $a^*(\lambda)$, Eq. 13 is now fitted to data on P^B_{max} on the one hand and on α^B on the other hand. The coefficients obtained are listed in Table 4. The vertical profiles of photophysiological parameters retrieved for the

Table 4. Parameters retrieved for the three phytoplankton classes (micro-, nano-, and picophytoplankton) by fitting Eq. 13 on P^B_{max} and α^B from database P-E. $x^*_{micro}(0)$, $x^*_{nano}(0)$, and $x^*_{pico}(0)$ are the values of P^B_{max} [mg C (mg Chl *a*)$^{-1}$ h^{-1}] or α^B [mg C (mg Chl *a*)$^{-1}$ h^{-1} (μmol quanta m^{-2} s^{-1})$^{-1}$] obtained for the surface ($z/Z_{eu} = 0$), and s_{micro}, s_{nano}, and s_{pico} are the slopes. For each parameter are given the estimate ± SE and the significance level (*$p < 0.05$; **$p < 0.01$; ***$p < 0.001$; ns: not significant). The correlation coefficient (r) and the root mean square error (RMSE) are also indicated.

	P^B_{max}		α^B	
$x^*_{micro}(0)$	4.26±0.45	***	0.032±0.007	***
s_{micro}	0.37±0.14	**	0.08±0.27	ns
$x^*_{micro}(0)$	2.94±0.43	***	0.026±0.005	***
s_{nano}	0.78±0.25	**	−0.67±0.23	**
$x^*_{micro}(0)$	3.75±0.37	***	0.007±0.003	*
s_{pico}	2.16±0.40	***	−1.26±0.45	**
r	0.603		0.418	
RMSE	1.11		0.020	

three phytoplankton classes are presented in Figs. 4b–f, and the reconstructed specific P versus E curves in Fig. 5.

The P^B_{max} specific to microphytoplankton is greater than that of the two other classes, with values comprised within the range 2.44–4.26 mg C (mg Chl *a*)$^{-1}$ h^{-1} within 0–1.5Z_{eu} versus 0.92–2.94 mg C (mg Chl *a*)$^{-1}$ h^{-1} for nano- and 0.15–3.75 mg C (mg Chl *a*)$^{-1}$ h^{-1} for picophytoplankton. The same trend is observed for Φ_{cmax} within the layer 0–0.8Z_{eu}, where Φ_{cmax} specific to micro- is higher [0.046–0.071 mol C (mol quanta)$^{-1}$] than that specific to nano- [0.021–0.047 mol C (mol quanta)$^{-1}$], itself higher than Φ_{cmax} specific to picophytoplankton [0.004–0.015 mol C (mol quanta)$^{-1}$]. Regarding α^B, values are greater for nanophytoplankton within the whole water column, except within the layer 0–0.3Z_{eu} where α^B specific to microphytoplankton is slightly superior [i.e., 0.032 vs. 0.028 mg C (mg Chl *a*)$^{-1}$ h^{-1} (μmol quanta m^{-2} s^{-1})$^{-1}$]. At the surface, retrieved values of E_k are much higher for picophytoplankton (i.e., 540 μmol quanta m^{-2} s^{-1}) than for the two other algal groupings (i.e., 133 for micro-, and 112 μmol quanta m^{-2} s^{-1} for nanophytoplankton). This trend vanishes as z/Z_{eu} increases because E_k specific to picophytoplankton exhibits a sharp decrease with depth (of a factor of about 30 within the euphotic layer), whereas E_k of micro- and nanophytoplankton remain more stable.

The strongest vertical gradients are observed for pico-, and the weakest for microphytoplankton, whatever the considered photophysiological property (note that for α^B s_{micro} is not significantly different from zero, Table 4; *see also* Fig. 5a,c). Those observed for nanophytoplankton usually stand between (cf. slopes listed in Table 4). For example, P^B_{max} experiences a nine-fold decrease from the surface down to Z_{eu} for picophytoplankton and decreases of a factor of 2.2 for nano- and of 1.5 for microphytoplankton. The Φ_{cmax} shows a 1.7-fold increase from Z_{eu} to the surface for microphytoplankton, whereas it increases by a factor of 2.8 and of 5.6 from the surface to Z_{eu} for nano- and picophytoplankton, respectively.

Malone (1980) reported a factor of 66 between extreme values of P^B_{max} associated with large phytoplankton and of 40 for values associated to medium- and small-sized phytoplankton. In a recent review on *Phaeocystis* (Schoemann et al. 2005), P^B_{max} was recorded to vary within a range of 0.2–22.5 mg C (mg Chl *a*)$^{-1}$ h^{-1}. Despite this, a wide range of variation in the photophysiological properties of algae is not the rule. Most of the studies carried out at sea or in the laboratory recorded values lying in a relatively narrow range, to which the present results compare favorably. For instance, Sarthou et al. (2005) reported a mean P^B_{max} of 2.6 ± 1.0 mg C (mg Chl *a*)$^{-1}$ h^{-1} in a review paper on diatoms, whereas P^B_{max} ranges within 2.6–5.6 mg C (mg Chl *a*)$^{-1}$ h^{-1} in Atlantic subtropical gyres (Marañon 2005) where algae assemblages are usually dominated by picophytoplankton. Our Φ_{cmax} values are consistent with those observed for a diatom bloom [e.g., 0.088 mol C (mol quanta)$^{-1}$; Cleveland et al. 1989], for a *Phaeocystis* bloom in Antarctic waters [e.g., 0.028–0.054 mol C (mol quanta)$^{-1}$; SooHoo et al. 1987], or for a small cells-dominated area [e.g., 0.007–0.025 mol C (mol quanta)$^{-1}$; Lindley et al. 1995].

Because of their dependence upon the light source used during the P versus E experiments, E_k and α^B cannot be rigorously compared to results from the literature. They are, nonetheless, consistent with those of Babin et al. (1996), whose data represent a small portion (6.5%) of database P-E. They actually reported α^B ranging within 0.013–0.088 mg C (mg Chl *a*)$^{-1}$ h^{-1} (μmol quanta m^{-2} s^{-1})$^{-1}$ and E_k within 20–400 μmol quanta m^{-2} s^{-1} in an oligotrophic system of the North Atlantic, and α^B varying around 0.025 mg C (mg Chl *a*)$^{-1}$ h^{-1} (μmol quanta m^{-2} s^{-1})$^{-1}$ and E_k around 180 μmol quanta m^{-2} s^{-1} in the Mauritanian upwelling.

Validity of the Chl a to diagnostic pigment ratios—The present analysis highlights that algal photophysiology is, in stratified oligotrophic systems in particular, strongly influenced by photoacclimation, which often results in changes in pigmentation and Chl *a* to pigment ratios. Therefore, estimating the [Chl *a*] associated with each of the three phytoplankton classes through Eqs. 6–8 and 10–12 would ideally require using a specific coefficient for each diagnostic pigment and for each depth (or layer of the water column). Such a procedure would be unmanageable when dealing with large datasets as it is the case here. Thus, we used coefficients derived from a global dataset and based on water-column integrated contents (Uitz et al. 2006). These coefficients should represent the best estimates of the average Chl *a* to diagnostic pigment ratios and have already proven to be valuable on meso- (Claustre et al. 2005) and large scales (Bricaud et al. 2004). Nevertheless, we may wonder whether they are relevant to ultimately parameterize the class-specific photophysiological properties and their depth-dependence.

To verify this assumption, we evaluated the impact of the Chl *a* to diagnostic pigment ratios on the retrieved photophysiological properties. A new set of coefficients was calculated by using individual samples (volumetric concentrations) collected in stratified waters within the

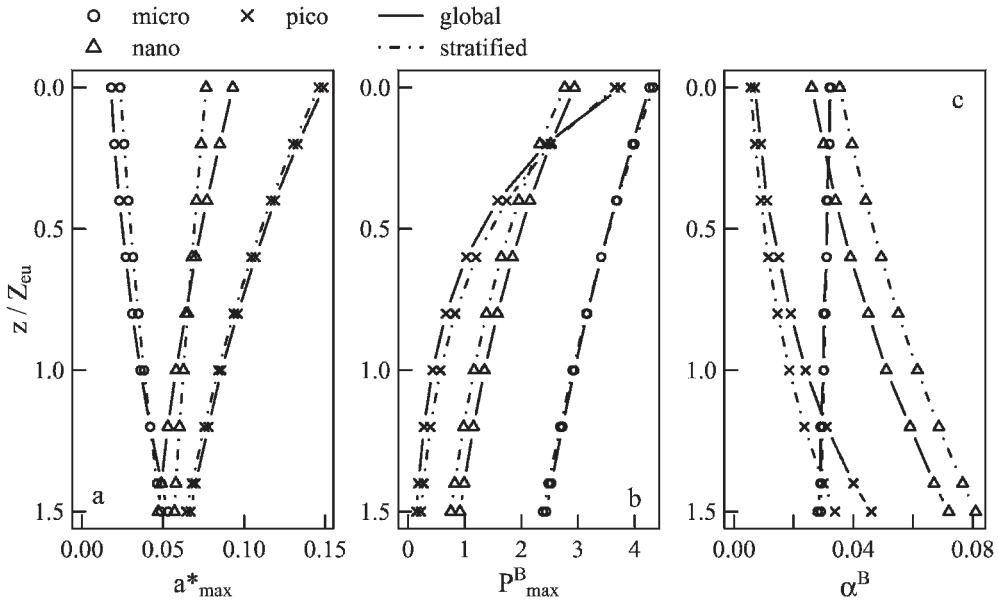

Fig. 6. Vertical profiles of the photophysiological properties specific to the three pigment-based size classes: micro- (circles), nano- (triangles), and picophytoplankton (crosses), obtained using the Chl *a* to diagnostic pigment ratios derived from either (i) the global dataset from Uitz et al. (2006) (global; solid lines), or (ii) the individual samples collected in stratified waters within the 0–1.5Z_{eu} layer (stratified; dashed lines). (a) a^*_{max} [m^2 (mg Chl *a*)$^{-1}$], (b) P^B_{max} [mg C (mg Chl *a*)$^{-1}$ h^{-1}], and (c) α^B [mg C (mg Chl *a*)$^{-1}$ h^{-1} (μmol quanta m^{-2} s^{-1})$^{-1}$].

layer 0–1.5Z_{eu}, similarly to the conditions of the present analysis. The equation obtained by multiple regression analysis was (n = 14,058, r^2 = 0.96, $p < 0.001$)

$$\begin{aligned}[\text{Chl}\,a] = {} & 1.65[\text{fucoxanthin}] + 1.30[\text{peridinin}] \\ & + 0.73[\text{alloxanthin}] + 0.78[19' - \text{BF}] \\ & + 0.83[19' - \text{HF}] + 1.29[\text{zeaxanthin}] \\ & + 0.77[\text{Chl}\,b + \text{divinyl} - \text{Chl}\,b]\end{aligned} \quad (14)$$

These coefficients were introduced in Eqs. 6–8 and 10–12 to estimate the Chl *a* biomass associated with each of the three phytoplankton classes. These new biomass estimates were, in turn, used to determine new phytoplankton class-specific spectral absorption coefficients and photosynthetic parameters.

The comparison of the resulting photophysiological properties to those obtained by using the ratios derived from the global dataset revealed no critical variations in the absolute values and no change in the class-specific trends (Fig. 6). Essentially, the maximum specific absorption coefficient showed an average variation of ±15% for micro-, ±11% for nano-, and ±3% for picophytoplankton. For P^B_{max}, the average variation was ±1% for micro-, ±12% for nano-, and ±24% for picophytoplankton. In the case of α^B, the average variation was ±2% for micro-, ±24% for nano-, and ±23% for picophytoplankton. The variations in the photophysiological properties specific to picophytoplankton were relatively small, though they are known to be influenced by photoacclimation. The most important variations were for nanophytoplankton, as a result of the increase in the coefficients attributed to their main biomarker pigments (19′-HF and 19′-BF). In particular, we observed a variation of 35% in the nano-specific α^B at surface, where the primary production is usually limited by P^B_{max}. Eventually, one can expect that the changes induced in the class-specific photophysiological properties do not have a significant impact on primary production.

This hypothesis was confirmed by comparing the class-specific and total primary production rates computed from the bio-optical model of Morel (1991) used in conjunction with either set of class-specific photophysiological properties (presented on Fig. 6) for a variety of environmental conditions. The class-specific [Chl *a*] profiles required for the calculation were inferred from the $[\text{Chl}\,a]_{surf}$ according to the procedure described in Uitz et al. (2006). The test was conducted for nine different $[\text{Chl}\,a]_{surf}$ values covering the trophic gradient 0.03–2.92 mg m^{-3} (i.e., the average $[\text{Chl}\,a]_{surf}$ of the nine trophic categories presented in Uitz et al. [2006]) at two contrasted latitudes (i.e., the Tropic of Cancer and 60°N), and two different seasons (i.e., June and December). Table 5 provides an example of the primary production rates computed for the Tropic of Cancer in June. For all of the situations, the variations in the column-integrated primary production retrieved by using either set of photophysiological properties were minor (ranging within ±0.1–7.7%).

Discussion

Dependence of photophysiological properties on the phytoplankton community composition—Our results on a large dataset representative of tropical and temperate

Table 5. Class-specific and total column-integrated primary production (g C m^{-2} d^{-1}) computed from the model of Morel (1991), used in conjunction with the class-specific photophysiological properties derived by using the Chl *a* to diagnostic pigment ratios based on either the global dataset from Uitz et al. (2006), or the individual samples collected in stratified waters within the layer 0–1.5Z_{eu} for nine $[\text{Chl } a]_{surf}$ values (mg m^{-3}) for the Tropic of Cancer in June. The total primary production rate is computed from the sum of the three class-specific primary production rates.

$[\text{Chl } a]_{surf}$	0.03	0.06	0.10	0.16	0.24	0.35	0.54	1.24	2.92
Using the ratios based on the global dataset									
P_{micro}	0.03	0.05	0.06	0.09	0.15	0.20	0.29	0.70	1.71
P_{nano}	0.11	0.13	0.15	0.19	0.25	0.29	0.31	0.34	0.37
P_{pico}	0.07	0.08	0.11	0.12	0.10	0.11	0.12	0.12	0.05
P_{total}	0.20	0.27	0.32	0.40	0.51	0.60	0.73	1.16	2.12
Using the ratios based on individual samples from stratified waters within the layer 0–1.5Z_{eu}									
P_{micro}	0.03	0.05	0.06	0.09	0.15	0.21	0.30	0.71	1.71
P_{nano}	0.10	0.12	0.14	0.18	0.23	0.26	0.29	0.32	0.35
P_{pico}	0.07	0.09	0.11	0.12	0.10	0.11	0.12	0.12	0.05
P_{total}	0.20	0.26	0.32	0.39	0.49	0.58	0.70	1.14	2.11

waters suggest that the three phytoplankton pigment-based size classes have specific photophysiological properties. In particular, microphytoplankton have higher light-saturated photosynthetic efficiency and maximum quantum yield for carbon fixation than the two other algal groupings (Figs. 4b,f and 5a). These results corroborate prior investigations reporting that microphytoplankton, and micro-dominated environments, present higher light-saturated photosynthetic efficiency (Cermeño et al. 2005), maximum quantum yield for carbon fixation (Babin et al. 1996; Lorenzo et al. 2005), cross section for photosynthesis (Claustre et al. 1997; Hashimoto and Shiomoto 2002; Claustre et al. 2005), and growth rate (Latasa et al. 2005). In addition, Marañon (2005) observed low growth rates of phytoplankton in Atlantic subtropical gyres typically dominated by picophytoplankton, which supports our findings. Our results are, however, contradictory to several studies showing that large phytoplankton are characterized by lower photosynthetic or growth yields than small ones (Laws et al. 1987; Bouman et al. 2005; Kameda and Ishizaka 2005) or suggesting no dependence of photophysiology on community structure at all (Finkel 2001).

Both trends can be justified based on metabolic theory and field or laboratory studies. On the one hand, the lower P^{B}_{max} observed in certain cases for microphytoplankton might be related to their inferior ability to assimilate nutrients and absorb light due to their lower surface to volume ratio (e.g., Malone 1980; Raven 1998). Thus, under conditions where the growth of smaller cells can be balanced, that of larger cells might be under nutrient stress and unbalanced. On the other hand, several arguments may explain why, as in the present study, microphytoplankton are characterized by higher P^{B}_{max} and Φ_{cmax}. Large phytoplankton, especially diatoms, are known to be mainly responsible for biomass increases (e.g., Margalef 1978; Malone 1980; Yentsch and Phinney 1989). Diatom blooms occur under favorable conditions (i.e., early stratification, nutrient-enriched waters), whereas, in contrast, picophytoplankton are present in stratified water columns with stable irradiance regimes and nutrient limitation. Beside this feature, diatoms, among other organisms, have evolved a nutrient storage vacuole conferring a competitive advantage to thrive in unstable environments (Malone 1980; Falkowski et al. 2004), which may partly balance the drawbacks due to their large size. Cermeño et al. (2005) also recently suggested that a higher photochemical efficiency of photosystem II may be responsible for higher P^{B}_{max} for large phytoplankton than for smaller ones. We may therefore wonder whether the higher P^{B}_{max} and Φ_{cmax} retrieved here for diatoms are caused by the favorable growth conditions they are usually associated with or related to actual intrinsic properties of these organisms.

As for the difference between nano- and picophytoplankton, based on the typical nutrient regime they experience, one may have expected picophytoplankton to have the lowest P^{B}_{max} of the three groups, especially close to surface. Instead our results indicate that nanoplankton present the lowest value of P^{B}_{max} within the 0–0.3Z_{eu} layer. This trend has to be related to photoacclimation and photoadaptation processes. Indeed, in stratified oligotrophic systems, the surface phytoplankton biomass is dominated by a high-light acclimated picoplankton population characterized by high E_k and, hence, high P^{B}_{max}.

As mentioned earlier, the photosynthetic parameters are subject to a variety of biological and physico-chemical factors, the influence of which cannot be discriminated in situ. It is very likely that the dominant factors controlling the photosynthetic parameters depend on the study region, season, and investigation scale. For instance, Claustre et al. (2005) observed significant correlations between photosynthetic parameters, light and temperature in the North Atlantic during summertime, as a result of phytoplankton acclimation. Those correlations no longer held true when considering the same region during winter or at the yearly scale. Similarly, Bouman et al. (2005) found a relationship between P^{B}_{max} and temperature for data collected on the Scotian Shelf, but no temperature-dependence for those collected in the Arabian Sea. The purpose of the present

study is to develop parameterizations applicable to large scales. In this context, the phytoplankton community structure that results from, and hence integrates, the combined influence of the various environmental factors appears as the most relevant indicator of the photophysiological properties. In that sense, the use of community structure is comparable to the use of biogeochemical provinces (Claustre et al. 1997). Indeed the continuum between strongly seasonal regimes characterizing the eutrophic systems to weakly seasonal regimes encountered in oligotrophic environments is equivalent to the continuum existing among community successions (Cullen et al. 2002).

Dependence of photophysiological properties on relative irradiance within the water column—As expected, the vertical patterns obtained for the photophysiological properties specific to the three phytoplankton groupings almost mimic those observed in environments where they prevail. Photophysiological properties specific to microphytoplankton display less vertical variability than those of the two other classes, as usually observed in eutrophic environments (e.g., Babin et al. 1996; Moran and Estrada 2001). The strong vertical gradients obtained for picophytoplankton, and to a lesser degree for nanophytoplankton, corroborate studies conducted in laboratory (e.g., review by MacIntyre et al. 2002), or in the field in stratified oligotrophic (e.g., Babin et al. 1996; Bouman et al. 2000) and mesotrophic (e.g., Lindley et al. 1995; Babin et al. 1996) regions. This vertical variability results from the photoacclimation and photoadaptation of algae to the irradiance field (Platt et al. 1980; Babin et al. 1996; Bouman et al. 2005), which is possible because typical timescales of vertical mixing are slower than those of acclimation processes (Cullen and Lewis 1988). As an example, high values of Φ_{cmax} encountered in deep waters are usually attributed to the reduced amount of non-photosynthetic pigments (e.g., Sosik 1996; Marra et al. 2000) and to a lesser extent to the availability of nutrients (Cleveland et al. 1989; Babin et al. 1996). The vertical distribution of E_k is consistent with its nature of photoacclimation status index (Sakshaug et al. 1997). Indeed, Table 3 showed that E_k is mainly correlated to the NPP index and to the proxy for relative irradiance z/Z_{eu}, as documented in studies conducted in stratified open-ocean regions (e.g., Babin et al. 1996; Bouman et al. 2000). High surface irradiances entail an increase in the photoprotectant pigment content, leading to a simultaneous increase in the NPP index and E_k. Regarding P^B_{max}, the vertical gradients may also be related to the normalization by the Chl *a* concentration (Behrenfeld et al. 2002*b*; MacIntyre et al. 2002). In such stratified oligotrophic systems, changes in photophysiological properties of algae are caused by modifications in the irradiance field (MacIntyre et al. 2002) in addition to community composition-related changes (Bouman et al. 2000).

Scope of applicability and perspectives—Predicting algal photophysiological properties on large to global scales is one of the unresolved issues we have to cope with to improve the modeled estimates of marine primary production (e.g., Morel et al. 1996; Behrenfeld et al. 2002*a*). Based on the analysis of two extensive datasets, this study introduces a hybrid approach in which the phytoplankton community composition, in conjunction with the relative irradiance within the water column, is used as an indicator of photophysiological properties. Relationships between algal photophysiology and community structure are not surprising. Algal photophysiology has already been suggested to be taxon- or size-dependent (e.g., Claustre et al. 1997; Hashimoto and Shiomoto 2002; Cermeño et al. 2005). In addition, the phytoplankton community structure is influenced by, and, thus, represents an integrator of environmental factors that control the photophysiological response of algae (Claustre et al. 2005). In that sense, the present approach may lead to an improvement of the prediction of photophysiological properties. This statement will need to be further tested and demonstrated in the future. Beside phytoplankton community composition, photoacclimation is another factor influencing algal photophysiological properties (e.g., MacIntyre et al. 2002). Photoacclimation processes affect particularly the photophysiological response of pico- and nanophytoplankton, which respectively dominate the biomass in stratified oligotrophic and mesotrophic systems. Therefore, it has to be accounted for to predict algal photophysiology in such environments.

Datasets including simultaneously collected HPLC measurements, P versus E curve parameters, and spectral absorption coefficients are still too rare. They constitute the essential tool required to investigate the role of community composition on algal photophysiology. The present approach relies on data collected from temperate and tropical regions and is thus only valid for those environments. If an application to the global scale is the ultimate goal, the proposed approach will need to be further evaluated and developed when expanded datasets become available. This especially holds true for the polar regions and the Arabian Sea, which were not account for here. Additional data sampled in low-latitude and temperate environments, during winter conditions and important productive events such as the North Atlantic spring bloom, could help strengthen general relationships. Finally, data from coastal productive waters would also be useful in the perspective of global applications. One of the main problems that remain is the dependence of the P versus E curve parameters (and of Φ_{cmax}) on measurement conditions (Sakshaug et al. 1997), which makes the merging of data collected by different laboratories difficult. The light-saturated photosynthetic rate (P^B_{max} or P^B_{opt}) has been reported to explain a large part of the variability of the column-integrated primary production (Balch and Byrne 1994; Behrenfeld and Falkowski 1997*b*) and is less dependent on the measurement conditions (Sakshaug et al. 1997). An interesting possibility could, thus, be to build an "as global as possible dataset" of simultaneous measurements of P^B_{max} (or P^B_{opt}) and HPLC-determined pigments.

At this time, fields of biomass specific to different phytoplankton types are becoming accessible from space (e.g., Sathyendranath et al. 2004; Alvain et al. 2005; Uitz et

al. 2006). If our results are confirmed, the proposed class-specific photophysiological properties could be incorporated in primary production models and used at the global scale. This approach may lead to an improvement of the estimate of primary production, traditionally based on a single phytoplankton variable. Furthermore, and perhaps more importantly, it will permit the conversion of class-specific biomass fields into fields of class-specific primary production rates. Such primary production fields are the first steps required for the validation and/or the parameterization of a new generation of biogeochemical models that explicitly integrate diverse phytoplankton types (e.g., Le Quéré et al. 2005).

References

Allali, K., A. Bricaud, and H. Claustre. 1997. Spatial variations in the chlorophyll-specific absorption coefficients of phytoplankton and photosynthetically active pigments in the equatorial Pacific. J. Geophys. Res. **102:** 12413–12423.

Alvain, S., C. Moulin, Y. Dandonneau, and F. M. Bréon. 2005. Remote sensing of phytoplankton groups in case I waters from global SeaWiFS imagery. Deep Sea Res. I **52:** 1989–2004.

Antoine, D., J. M. André, and A. Morel. 1996. Oceanic primary production 2. Estimation at global scale from satellite (coastal zone color scanner) chlorophyll. Global Biogeochem. Cycles **10:** 57–69.

Babin, M., A. Morel, H. Claustre, A. Bricaud, Z. S. Kolber, and P. G. Falkowski. 1996. Nitrogen- and irradiance-dependent variations of the maximum quantum yield of carbon fixation in eutrophic, mesotrophic and oligotrophic marine systems. Deep-Sea Res. I **43:** 1241–1272.

———, ———, and R. Gagnon. 1994. An incubator designed for extensive and sensitive measurements of phytoplankton photosynthetic parameters. Limnol. Oceanogr. **39:** 694–702.

Balch, W. M., and C. F. Byrne. 1994. Factors affecting the estimate of primary production from space. J. Geophys. Res. **99:** 7555–7570.

Behrenfeld, M. J., W. E. Esaias, and K. R. Turpie. 2002a. Assessment of primary production at the global scale, p. 156–186. *In* P. J. le B. Williams, D. N. Thomas and R. A. Reynolds [eds.], Phytoplankton productivity: Carbon assimilation in marine and freshwater ecosystems. Blackwell.

———, and P. G. Falkowski. 1997*a*. A consumer's guide to phytoplankton primary productivity models. Limnol. Oceanogr. **42:** 1479–1491.

———, and ———. 1997*b*. Photosynthetic rates derived from satellite-based chlorophyll concentration. Limnol. Oceanogr. **42:** 1–20.

———, E. Maranon, D. A. Siegel, and S. B. Hooker. 2002*b*. Photoacclimation and nutrient-based model of light-saturated photosynthesis for quantifying oceanic primary production. Mar. Ecol. Prog. Ser. **228:** 103–117.

Bidigare, R. R., M. E. Ondrusek, J. H. Morrow, and D. A. Kiefer. 1990. In vivo absorption properties of algal pigments. Ocean Optics 10, SPIE **1302:** 290–302.

Bouman, H. A., T. Platt, G. W. Kraay, S. Sathyendranath, and B. D. Irwin. 2000. Bio-optical properties of the subtropical North Atlantic. 1. Vertical variability. Mar. Ecol. Prog. Ser. **200:** 3–18.

———, ———, S. Sathyendranath, W. K. W. Li, V. Stuart, C. Fuentes-Yaco, H. Maass, E. P. W. Horne, O. Ulloa, V. A. Lutz, and M. Kyewalyanga. 2003. Temperature as indicator of optical properties and community structure of marine phytoplankton: Implications for remote sensing. Mar. Ecol. Prog. Ser. **258:** 19–30.

———, ———, ———, and V. Stuart. 2005. Dependence of light-saturated photosynthesis on temperature and community structure. Deep-Sea Res. I **52:** 1284–1299.

———, and others. 2006. Oceanographic basis of the global surface distribution of *Prochlorococcus* ecotypes. Science **312:** 918–921.

Bricaud, A., H. Claustre, J. Ras, and K. Oubelkheir. 2004. Natural variability of phytoplankton absorption in oceanic waters: Influence of the size structure of algal populations. J. Geophys. Res. **109:** C11010, doi:10.1029/2004JC002419.

———, A. Morel, M. Babin, K. Allali, and H. Claustre. 1998. Variations of light absorption by suspended particles with chlorophyll a concentration in oceanic (case 1) waters: Analysis and implications for bio-optical models. J. Geophys. Res. **103:** 31033–31044.

Cermeño, P., P. Estévez-Blanco, E. Marañon, and E. Fernandez. 2005. Maximum photosynthetic efficiency of size-fractionated phytoplankton assessed by ^{14}C uptake and fast repetition rate fluorometry. Limnol. Oceanogr. **50:** 1438–1446.

Chisholm, S. W. 1992. Phytoplankton size. p. 213–237. *In* P. G. Falkowski and A. D. Woodhead [eds.], Primary productivity and biogeochemical cycles in the sea. Plenum.

Ciotti, A. M., M. R. Lewis, and J. J. Cullen. 2002. Assessment of the relationships between dominant cell size in natural phytoplankton communities and the spectral shape of the absorption coefficient. Limnol. Oceanogr. **47:** 404–417.

Claustre, H. 1994. The trophic status of various oceanic provinces as revealed by phytoplankton pigment signatures. Limnol. Oceanogr. **39:** 1206–1210.

———, and J. C. Marty. 1995. Specific phytoplankton biomasses and their relation to primary production in the Tropical North Atlantic. Deep-Sea Res. I **42:** 1475–1493.

———, M. A. Moline, and B. B. Prezelin. 1997. Sources of variability in the column photosynthetic cross section for Antarctic coastal waters. J. Geophys. Res. **102:** 25047–25060.

———, and others. 2005. Towards a taxon-specific parameterization of bio-optical models of primary production: A case study in the North Atlantic. J. Geophys. Res. **110:** C07S12, doi:10.1029/2004JC002634.

Cleveland, J. S., M. J. Perry, D. A. Kiefer, and M. C. Talbot. 1989. Maximal quantum yield of photosynthesis in the northwestern Sargasso Sea. J. Mar. Res. **47:** 869–886.

Côté, B., and T. Platt. 1983. Day-to-day variations in the spring-summer photosynthetic parameters of coastal marine phytoplankton. Limnol. Oceanogr. **28:** 320–344.

Cullen, J. J., P. J. S. Franks, D. M. Karl, and A. R. Longhurst. 2002. Physical influences on marine ecosystem dynamics, p. 297–336. *In* A. R. Robinson, J. J. McCarthy and B. J. Rothschild [eds.], The sea. Wiley.

———, and M. R. Lewis. 1988. The kinetics of algal photoadaptation in the context of vertical mixing. J. Plankton Res. **10:** 1039–1063.

de Boyer Montégut, C., G. Madec, A. S. Fischer, A. Lazar, and D. Iudicone. 2004. Mixed layer depth over the global ocean: An examination of profile data and a profile-based climatology. J. Geophys. Res. **109:** C12003, doi:10.1029/2004JC002378.

Devred, E., S. Sathyendranath, V. Stuart, H. Maass, O. Ulloa, and R. Platt. 2006. A two-component model of phytoplankton absorption in the open-ocean: Theory and applications. J. Geophys. Res. **111:** C03011, doi:10.1029/2005JC002880.

Eppley, R. W., and B. J. Peterson. 1979. Particulate organic matter flux and planktonic new production in the deep ocean. Nature **282:** 677–680.

Falkowski, P. G., and J. A. Raven. 1997. Aquatic photosynthesis in biogeochemical cycles. p. 300–335. *In* P. G. Falkowski and J. A. Raven [eds.], Aquatic photosynthesis. Blackwell Science.

———, and Others. 2004. The evolution of modern eukaryotic phytoplankton. Science **305:** 354–360.

Finkel, Z. V. 2001. Light absorption and size scaling of light-limited metabolism in marine diatoms. Limnol. Oceanogr. **46:** 86–94.

Frenette, J. J., S. Demers, L. Legendre, and J. Dodson. 1993. Lack of agreement among models for estimating the photosynthetic parameters. Limnol. Oceanogr. **38:** 679–687.

Gibb, S. W., D. G. Cummings, X. Irigoien, R. G. Barlow, R. Fauzi, and C. Mantoura. 2001. Phytoplankton pigment chemotaxonomy of the northeastern Atlantic. Deep-Sea Res. II **48:** 795–823.

Gieskes, W. W. C., G. W. Kraay, A. Nontji, D. Setiapermana, and D. Sutomo. 1988. Monsoonal alternation of a mixed and a layered structure in the phytoplankton of the euphotic zone of the Banda Sea (Indonesia): A mathematical analysis of algal pigment fingerprints. Neth. J. Sea Res. **22:** 123–137.

Goldman, J. C. 1993. Potential role of large oceanic diatoms in new primary production. Deep-Sea Res. I **40:** 159–168.

Hashimoto, S., and A. Shiomoto. 2002. Light utilization efficiency of size-fractionated phytoplankton in the subarctic Pacific, spring and summer 1999: High efficiency of large-sized diatom. J. Plankton Res. **24:** 83–87.

Hiscock, M. R., and others. 2003. Primary productivity and its regulation in the Pacific Sector of the Southern Ocean. Deep-Sea Res. II **50:** 533–558.

Hoepffner, N., and S. Sathyendranath. 1991. Effect of pigment composition on absorption of phytoplankton. Mar. Ecol. Prog. Ser. **73:** 11–23.

Kameda, T., and J. Ishizaka. 2005. Size-fractionated primary production estimated by a two-phytoplankton community model applicable to ocean color remote sensing. J. Oceanogr. **61:** 663–672.

Kana, T. M., P. M. Glibert, R. Goericke, and N. A. Welschmeyer. 1988. Zeaxanthin and β-carotene in *Synechococcus* WH7803 respond differently to irradiance. Limnol. Oceanogr. **33:** 1623–1627.

Kiorbe, T. 1993. Turbulence, phytoplankton cell size, and the structure of pelagic food webs. Adv. in Mar. Biol. **29**.

Latasa, M., X. A. G. Moran, R. Scharek, and M. Estrada. 2005. Estimating the carbon flux through main phytoplankton groups in the northwestern Mediterranean. Limnol. Oceanogr. **50:** 1447–1458.

Laws, E. A., G. R. DiTullio, and D. G. Redalje. 1987. High phytoplankton growth and production rates in the North Pacific subtropical gyre. Limnol. Oceanogr. **32:** 905–918.

Legendre, L., and J. Le Fevre. 1989. Hydrodynamic control of marine phytoplankton production, p. 49–63. *In* W. H. Berger, V. Smetacek and G. Wefer [eds.], Productivity of the ocean: Present and past. Wiley.

Le Quéré, C., and others. 2005. Ecosystem dynamics based on plankton functional types for global ocean biogeochemistry models. Global Change Biol. **11:** 2016–2040.

Lindley, S. T., R. R. Bidigare, and R. T. Barber. 1995. Phytoplankton photosynthesis parameters along 140 degree W in the Equatorial Pacific. Deep-Sea Res. II **42:** 441–463.

Lohrenz, S. E., A. D. Weidemann, and M. Tuel. 2003. Phytoplankton spectral absorption as influenced by community size structure and pigment composition. J. Plankton Res. **25:** 35–61.

Longhurst, A. R. 1995. Seasonal cycles of pelagic production and consumption. Prog. Oceanogr. **36:** 77–167.

———, S. Sathyendranath, T. Platt, and C. M. Caverhill. 1995. An estimate of global primary production in the ocean from satellite radiometer data. J. Plankton Res. **17:** 1245–1271.

Lorenzo, L. M., B. Arbones, G. H. Tilstone, and F. G. Figueiras. 2005. Across-shelf variability of phytoplankton composition, photosynthetic parameters and primary production in the NW Iberian upwelling system. J. Mar. Syst. **54:** 157–173.

Lutz, V. A., S. Sathyendranath, E. J. H. Head, and W. K. W. Li. 2003. Variability in pigment composition and optical characteristics of phytoplankton in the Labrador Sea and the Central North Atlantic. Mar. Ecol. Prog. Ser. **260:** 1–18.

MacIntyre, H. L., T. M. Kana, T. Anning, and R. J. Geider. 2002. Photoacclimatation of photosynthesis irradiance response curves and photosynthetic pigments in microalgae and cyanobacteria. J. Phycol. **38:** 17–38.

Malone, T. C. 1980. Algal size. p. 433–463. *In* I. Morris [ed.], The physiological ecology of phytoplankton. Univ. California.

Marañon, E. 2005. Phytoplankton growth rates in the Atlantic subtropical gyres. Limnol. Oceanogr. **50:** 299–310.

———, and P. M. Holligan. 1999. Photosynthetic parameters of phytoplankton from 50 degree N to 50 degree S in the Atlantic Ocean. Mar. Ecol. Prog. Ser. **176:** 191–203.

Margalef, R. 1965. Ecological correlation and relationship between primary producing and plankton structure. Mem. Ist. Ital. Idrobiol. **18:** 355–364.

———. 1978. Life-forms of phytoplankton as survival alternatives in an unstable environment. Oceanol. Acta **1:** 493–509.

Marra, J., C. C. Trees, R. R. Bidigare, and R. T. Barber. 2000. Pigment absorption and quantum yields in the Arabian Sea. Deep-Sea Res. II **47:** 1279–1299.

Moline, M. A., and B. B. Prézelin. 1996. Long-term monitoring and analyses of physical factors regulating variability in coastal Antarctic phytoplankton biomass, in situ productivity and taxonomic composition over subseasonal, seasonal and interannual time scales. Mar. Ecol. Prog. Ser. **145:** 143–160.

Moore, L. R., and S. W. Chisholm. 1999. Photophysiology of the marine cyanobacterium *Prochlorococcus*: Ecotypic differences among cultured isolates. Limnol. Oceanogr. **44:** 628–638.

———, R. Goericke, and S. W. Chisholm. 1995. Comparative physiology of *Synechococcus* and *Prochlorococcus*: Influence of light and temperature on growth, pigments, fluorescence and absorptive properties. Mar. Ecol. Prog. Ser. **116:** 259–275.

Moran, X. A. G., and M. Estrada. 2001. Short-term variability of photosynthetic parameters and particulate and dissolved primary production in the Alboran Sea (SW Mediterranean). Mar. Ecol. Prog. Ser. **212:** 53–67.

Morel, A. 1991. Light and marine photosynthesis: a spectral model with geochemical and climatological implications. Prog. Oceanogr. **26:** 263–306.

———, Y. H. Ahn, F. Partensky, D. Vaulot, and H. Claustre. 1993. *Prochlorococcus* and *Synechococcus*: A comparative study of their optical properties in relation to their size and pigmentation. J. Mar. Res. **51:** 617–649.

———, D. Antoine, M. Babin, and Y. Dandonneau. 1996. Measured and modeled primary production in the Northeast Atlantic (EUMELI JGOFS program): The impact of natural variations in photosynthetic parameters on model predictive skill. Deep-Sea Res. I **43:** 1273–1304.

———, and A. Bricaud. 1981. Theoretical results concerning light absorption in a discrete medium, and application to specific absorption of phytoplankton. Deep-Sea Res. **28:** 1375–1393.

———, and S. Maritorena. 2001. Bio-optical properties of oceanic waters: A reappraisal. J. Geophys. Res. **106:** 7163–7180.

Partensky, F., J. Blanchot, and D. Vaulot. 1999*a*. Differential distribution and ecology of *Prochlorococcus* and *Synechococcus* in oceanic waters: A review, p. 457–475. *In* L. Charpy and A. W. D. Larkum [eds.], Marine cyanobacteria. Institute of Oceanography Monaco.

———, W. R. Hess, and D. Vaulot. 1999*b*. *Prochlorococcus*, a marine photosynthetic prokaryote of global significance. Microbiol. Mol. Biol. Rev. **63:** 107–127.

———, N. Hoepffner, W. K. W. Li, O. Olloa, and D. Vaulot. 1993. Photoacclimation of *Prochlorococcus* sp. (Prochlorophyta) strains isolated from North Atlantic and Mediterranean Sea. Plant Physiol. **101:** 285–296.

Platt, T., C. L. Gallegos, and W. G. Harrison. 1980. Photoinhibition of photosynthesis in natural assemblages of marine phytoplankton. J. Mar. Res. **38:** 687–701.

Raven, J. A. 1998. Small is beautiful: The picophytoplankton. Funct. Ecol. **12:** 503–513.

Sakshaug, E., K. Andresen, and D. A. Kiefer. 1989. A steady state description of growth and light absorption in the marine planktonic diatom *Skeletonema costatum*. Limnol. Oceanogr. **34:** 198–205.

———, and others. 1997. Parameters of photosynthesis: Definitions, theory and interpretation of results. J. Plankton Res. **19:** 1637–1670.

Sarthou, G., K. R. Timmermans, S. Blain, and P. Tréguer. 2005. Growth physiology and fate of diatoms in the ocean: A review. J. Sea Res. **53:** 25–42.

Sathyendranath, S., L. Lazzara, and L. Prieur. 1987. Variations in the spectral values of specific absorption of phytoplankton. Limnol. Oceanogr. **32:** 403–415.

———, A. R. Longhurst, C. M. Caverhill, and T. Platt. 1995. Regionally and seasonally differentiated primary production in the North Atlantic. Deep-Sea Res. I **42:** 1773–1802.

———, L. Watts, E. Devred, T. Platt, C. M. Caverhill, and H. Maass. 2004. Discrimination of diatom from other phytoplankton using ocean-colour data. Mar. Ecol. Prog. Ser. **272:** 59–68.

Scharek, R., M. Latasa, D. M. Karl, and R. R. Bidigare. 1999. Temporal variations in diatom abundance and downward vertical flux in the oligotrophic North Pacific Gyre. Deep-Sea Res. I **46:** 1051–1075.

Schoemann, V., S. Becquevort, J. Stefels, V. Rousseau, and C. Lancelot. 2005. *Phaeocystis* blooms in the global ocean and their controlling mechanisms: A review. J. Sea Res. **53:** 43–66.

Six, C., J. C. Thomas, B. Brahamsha, Y. Lemoine, and F. Partensky. 2004. Photophysiology of the marine cyanobacterium *Synechococcus* sp. WH8102, a new model organism. Aquat. Microb. Ecol. **35:** 17–29.

Soohoo, J. B., A. C. Palmisano, S. T. Kottmeier, M. P. Lizotte, S. L. Soohoo, and C. W. Sullivan. 1987. Spectral light absorption and quantum yield of photosynthesis in sea ice microalagae and a bloom of *Phaeocystis pouchetii* from McMurdo Sound, Antarctica. Mar. Ecol. Prog. Ser. **39:** 175–189.

Sorensen, J. C., and D. A. Siegel. 2001. Variability of the effective quantum yield for carbon assimilation in the Sargasso Sea. Deep-Sea Res. II **48:** 2005–2035.

Sosik, H. M. 1996. Bio-optical modelling of primary production: Consequences of variability in quantum yield and specific absorption. Mar. Ecol. Prog. Ser. **143:** 225–238.

———, and B. G. Mitchell. 1995. Light absorption by phytoplankton, photosynthetic pigments and detritus in the California Current System. Deep-Sea Res. I **42:** 1717–1748.

Stramski, D., A. Sciandra, and H. Claustre. 2002. Effects of temperature, nitrogen, and light limitation on the optical properties of the marine diatom *Thalassiosira pseudonana*. Limnol. Oceanogr. **47:** 392–403.

Sukenik, A., J. Bennett, and P. G. Falkowski. 1987. Light-saturated photosynthesis—limitation by electron transport or carbon fixation? Biochim. Biophys. Acta **891:** 205–215.

Uitz, J., H. Claustre, A. Morel, and S. B. Hooker. 2006. Vertical distribution of phytoplankton communities in open ocean: An assessment based on surface chlorophyll. J. Geophys. Res. **111:** C08005, doi:10.1029/2005JC003207.

Van Heukelem, L., and C. S. Thomas. 2001. Computer-assisted high-performance liquid chromatography method development with applications to the isolation and analysis of phytoplankton pigments. J. Chromatography A **910:** 31–49.

Vidussi, F., H. Claustre, J. Bustillos-Guzman, C. Cailliau, and J. C. Marty. 1996. Rapid HPLC method for determination of phytoplankton chemotaxinomic pigments: Separation of chlorophyll a from divinyl-chlorophyll a and zeaxanthin from leutein. J. Plankton Res. **18:** 2377–2382.

———, ———, B. B. Manca, A. Luchetta, and J. C. Marty. 2001. Phytoplankton pigment distribution in relation to upper thermocline circulation in the eastern Mediterranean Sea during winter. J. Geophys. Res. **106:** 19939–919956.

Wozniak, B., J. Dera, D. Ficek, R. Majchrowski, M. Ostrowska, and S. Kaczmarek. 2003. Modeling light and photosynthesis in the marine environment. Oceanologia **45:** 171–245.

———, ———, ———, M. Ostrowska, and R. Majchrowski. 2002. Dependence of the photosynthesis quantum yield in oceans on environmental factors. Oceanologia **44:** 439–459.

Yentsch, C., and D. Phinney. 1989. A bridge between ocean optics and microbial ecology. Limnol. Oceanogr. **34:** 1694–1705.

Received: 9 January 2007
Accepted: 7 October 2007
Amended: 30 October 2007